PHOTONICS Research

Highly efficient generation of arbitrary vector beams with tunable polarization, phase, and amplitude

Sheng Liu,† Shuxia Qi,† Yi Zhang, Peng Li, Dongjing Wu, Lei Han, and Jianlin Zhao*

MOE Key Laboratory of Material Physics and Chemistry under Extraordinary Conditions, and Shaanxi Key Laboratory of Optical Information Technology, School of Science, Northwestern Polytechnical University, Xi'an 710129, China
**Corresponding author: jlzhao@nwpu.edu.cn*

Received 14 November 2017; revised 21 January 2018; accepted 23 January 2018; posted 24 January 2018 (Doc. ID 313394); published 1 March 2018

We propose an efficient and robust method to generate tunable vector beams by employing a single phase-type spatial light modulator (SLM). With this method, a linearly polarized Gaussian beam can be converted into a vector beam with arbitrarily controllable polarization state, phase, and amplitude. The energy loss during the conversion is greatly reduced and depends mainly on the reflectivity of the SLM. We experimentally demonstrate that conversion efficiency of about 47% is achieved by using an SLM with reflectivity of 62%. Several typical vector beams, including cylindrical vector beams, vector beams on higher order Poincaré spheres, and arbitrary vector beams attached with phases and with tunable amplitude, are generated and verified experimentally. This method is also expected to create high-power vector beams and play important roles in optical fabrication and light trapping.

OCIS codes: (260.5430) Polarization; (260.6042) Singular optics; (070.6120) Spatial light modulators.

https://doi.org/10.1364/PRJ.6.000228

1. INTRODUCTION

In recent years, a new class of laser beams characterized by space-variant polarization states, also named vector beams, has become a popular topic [1]. The most dramatic one is the cylindrical vector beam (CVB) with cylindrical symmetry in polarization distribution [2], due to unique focusing properties [3,4]. The focal fields of CVBs can be robustly controlled when modulated radially [5–7] and azimuthally [8–10], or even attached with additional phase [9–11]. Meanwhile, vector beams with different spatial polarization distributions are successively presented with the purpose of characterizing optical orbital angular momentum [12–15], realizing spin-dependent propagation [16–19], and achieving spin–orbital interaction [20–22]. Moreover, vector beams have been exploited in many scientific and engineering applications, such as optical trapping [23,24], super-resolution microscopy [25], and laser micromachining [26,27].

To generate vector beams, a great number of schemes and systems have been developed. One of them, usually called the direct method, is to directly transform the polarization state of a traditional laser mode into a space-variant one by using designed optical elements, such as axial birefringent components [28], Brewster angle reflectors [29], spatially varying retarders [30,31], subwavelength gratings [32], and metasurfaces [33,34]. These direct methods often have high conversion efficiencies. However, the corresponding optical elements require special fabrication techniques, and they lack flexibility and convenience. Even when the controllable schemes based on the spatially varying retarders are proposed [35–37], they are applied only to creating a specific type of vector beam, e.g., higher order Poincaré sphere beams [36,37]. To conveniently control the space-variant polarization state of a light beam, many optical arrangements containing spatial light modulators (SLMs) have been presented [1,16,38–45], on the grounds of the superposition principle with orthogonal polarization components. In these superposition methods (also called indirect methods), it is required to impart the desired phases to the orthogonal polarization components, which are exactly implemented with a computer-generated hologram, or a more efficient phase-type SLM. However, the general low efficiency of generating vector beams with superposition methods leads to waste of energy. For example, in Refs. [1,41,45], where the phase-type SLM works as a pair of screens, at least 75% of the beam energy is lost irrespective of the loss from the SLM, because the beam passes through a beam splitter twice. Of course, efficiency can be greatly improved if the phase-modulated elements are replaced with elements such as space-variant phase plates [46] and polarization holograms [47], but it also leads to the loss of flexibility.

In this paper, we propose an optical arrangement containing a single phase-type SLM to generate vector beams, of which the polarization states, phases, and amplitudes can be arbitrarily controlled. The energy loss of this arrangement is greatly reduced and the generating efficiency is improved substantially.

2. EXPERIMENTAL SETUP

Generally, a vector beam is considered a superposition of two polarization components with respect to the orthonormal circular polarization basis $\{\boldsymbol{e}_L, \boldsymbol{e}_R\}$ [38,42], of which the Jones vectors are $[1, \pm i]^T/\sqrt{2}$. We can construct the vector beam by modulating its two polarization components separately. The experimental setup is shown in Fig. 1. A horizontally polarized input laser beam (He–Ne laser, 632.8 nm), with its Jones vector $[1, 0]^T$, passes through a half-wave plate (HWP, fast axis along an angle $\theta \in [0, \pi/2]$), and its polarization is changed into a linear one $[\cos 2\theta, \sin 2\theta]^T$. This linearly polarized beam is split into horizontally and vertically polarized components (i.e., p- and s-components) via a triangular common-path interferometer (TCPI), which is comprised of a polarizing beam splitter and two mirrors. The p- and s-components ($[\cos 2\theta, 0]^T$, $[0, \sin 2\theta]^T$), which propagate parallel to each other, are reflected to a phase-type SLM (Holoeye LETO) by one face of a right-angle prism mirror (RAPM), and respectively illuminate the left and right halves of the SLM screen, where two different phase patterns (Φ_1 and Φ_2) are addressed. After that, the p- and s-components, $[\cos 2\theta \exp(i\Phi_1), 0]^T$ and $[0, \sin 2\theta \exp(i\Phi_2)]^T$, are reflected by the other face of the RAPM and are recombined and superposed coaxially by another TCPI. Finally, the two components are converted to orthonormal circular polarizations via a quarter-wave plate (with its fast axis along 45°) and are synthesized to a vector beam, of which the polarization is given by

$$|\boldsymbol{E}\rangle = \cos 2\theta e^{i(\Phi_1+\delta_\Phi)}\boldsymbol{e}_R + \sin 2\theta e^{i\Phi_2}\boldsymbol{e}_L, \tag{1}$$

where the phase difference δ_Φ between the two components is generated from the asymmetry of this system. Since this phase difference can be compensated by appending a constant phase to the phase pattern of Φ_1, it is negligible in Eq. (1) and can be written as a constant, i.e., $\delta_\Phi = 0$, for convenience. Thus the polarization of the vector beam is written as

$$|\boldsymbol{E}\rangle = e^{i\Psi}\boldsymbol{T}(-\Theta)\begin{bmatrix}\cos\left(2\theta-\frac{\pi}{4}\right)\\ i\sin\left(2\theta-\frac{\pi}{4}\right)\end{bmatrix}, \tag{2}$$

where

$$\Psi = (\Phi_1 + \Phi_2)/2, \tag{3a}$$

$$\Theta = (\Phi_1 - \Phi_2)/2, \tag{3b}$$

$$\boldsymbol{T}(\Theta) = \begin{bmatrix}\cos\Theta & \sin\Theta\\ -\sin\Theta & \cos\Theta\end{bmatrix}. \tag{3c}$$

In Eq. (2), the Jones vector denotes an elliptical polarization with horizontal principal axis, and the axis ratio is $\cot(2\theta - \pi/4)$; the matrix $\boldsymbol{T}(-\Theta)$ denotes an anticlockwise rotation operation on this elliptical polarization with rotation angle Θ; Ψ is the additional phase. Namely, Eq. (2) represents a vector beam attached with a phase Ψ, and the polarization distribution satisfies: the principal axis is along angle Θ, and the ellipticity is $\cot(2\theta - \pi/4)$.

Mostly, the two circularly polarized components are set with equal intensity so that the resulting field is locally linearly polarized, which is associated with the general CVBs. In this case, $\theta = \pi/8$, and the output polarization is expressed as

$$|\boldsymbol{E}\rangle = e^{i\Psi}\begin{bmatrix}\cos\Theta\\ \sin\Theta\end{bmatrix}. \tag{4}$$

The resulting vector beam is captured by a CCD camera. To exactly observe the output polarization, a lens is used to image the light field at the plane of the SLM to the CCD. To examine the polarization and phase of the vector beam, we employ the method based on Pancharatnam–Berry phase (PB-phase method) that we recently proposed [48].

To reduce the energy loss during the mode conversion, we use beam splitting and combining systems in our setup, which are two TCPIs that include polarizing beam splitters, as also shown in Fig. 1. The p- and s-components can separately propagate with little loss at each face of the splitters. Importantly, the SLM responds only for a horizontally polarized beam, so it is necessary to set an HWP closely before the half screen of the SLM to transform the polarization of the s-component to horizontal. Of course, it can be transformed back to vertical polarization by the same HWP after it is granted phase Φ_1. In this arrangement, we measure the transmittance of the major elements, and find that 89% of the beam energy can pass through the TCPI, while 62% passes through the SLM when loading a null phase map. Finally, this setup gets a transmittance of about 47%. It has to be emphasized that the most energy loss comes from the SLM used here. If a highly reflective SLM is employed, the transmittance would be greatly improved.

This arrangement also possesses a promising ability to generate a femtosecond vector beam, which has been proposed to fabricate and manipulate complex morphologies [49]. In this

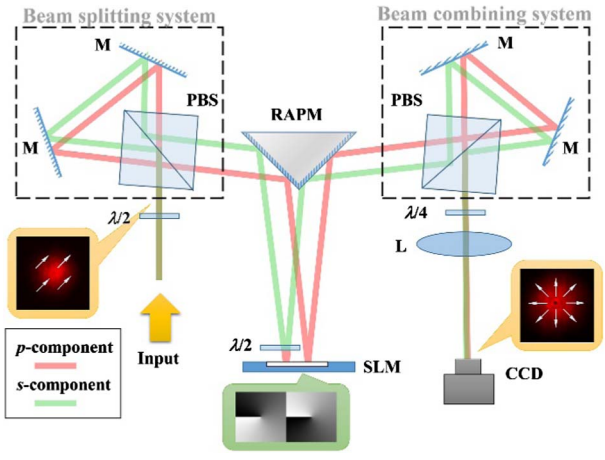

Fig. 1. Experimental setup for generating arbitrary vector beams. $\lambda/2$, half-wave plate; PBS, polarizing beam splitter; M, mirror; RAPM, right-angle prism mirror; SLM, phase-type spatial light modulator; $\lambda/4$, quarter-wave plate; L, lens. The elements enclosed in the dashed boxes compose triangular common-path interferometers.

scheme, all the optical elements should be replaced by achromatic ones, and the SLM can optionally be LCOS-SLM (Hamamatsu×11840 – 02) with reflectivity of 94%. Theoretically, a femtosecond laser pulse (800 nm, 50 fs) with a maximum power of 2.73 W can be withstood, and can be converted to the vector beam with an efficiency of about 71%.

On the other hand, the beam splitting and combining systems in the arrangement can also be achieved by two beam displacers, which have nearly the same transmittance as the TCPI. The beam displacers facilitate setting up the optical system and stabilize it further. However, due to the aperture limitation of the beam displacers, the waist of the input beam needs to be limited.

3. EXPERIMENTAL RESULTS AND DISCUSSION

A. Generating Cylindrical Vector Beams

To generate pure CVBs via the setup shown in Fig. 1, we set $\theta = \pi/8$, $\Psi = 0$, and $\Theta = \varphi + \varphi_0$, where φ is the coordinate of the azimuthal angle, and φ_0 is a constant equal to the angle between the polarization orientation of the CVB and the radial coordinate. Therefore, the phase patterns loaded on the SLM meet $\Phi_1 = -\Phi_2 = \varphi + \varphi_0$. Notably, there exist inevitable phase errors that the beam obtains from the SLM, which leads to the emergence of dark lines of light intensity at the boundary of phases 0 and 2π. To solve this problem, we attach the same phase grating ($\varphi_g = k_x x$, where k_x is a constant) to the phase patterns of Φ_1 and Φ_2, i.e., $\Phi_1 = \varphi + \varphi_0 + \varphi_g$, $\Phi_2 = -\varphi - \varphi_0 + \varphi_g$. Then, a spatial filter is set at the focal plane of the imaging lens to let only the first order pass through. This operation leads to a slight diminution of the transmittance of the setup. The transmittance is about 45% in our experiment.

Figure 2 shows the experimental results of the radially (the first column) and azimuthally (the second column) polarized beams generated by the setup of Fig. 1; Fig. 2(a) shows the intensity patterns captured by the CCD. It can be seen that dark points appear at the center of light spots caused by the singularity of polarization. The polarizations of these two vector beams are measured with the PB-phase method [48], and the results are shown in Figs. 2(b)–2(d), which depict the normalized Stokes parameters (S_1, S_2, S_3), respectively. The Jones vectors of the radially and azimuthally polarized beams are $[\cos\varphi, \sin\varphi]^T$ and $[-\sin\varphi, \cos\varphi]^T$, respectively. The corresponding Stokes parameters are $(\cos 2\varphi, \sin 2\varphi, 0)$ and $(-\cos 2\varphi, -\sin 2\varphi, 0)$, respectively. In contrast to this theory, the measured Stokes parameters characterize well the states of radial and azimuthal polarizations. To represent the measured polarization states more visually, the polarization ellipses are calculated with the data of the Stokes parameters, as depicted in Fig. 2(e). These results perfectly present the radial and azimuthal polarizations in the center regions of the light fields, while in the dark regions, elliptical polarizations appear due to measurement errors.

B. Generating Vector Beams on a Higher Order Poincaré Sphere

If we set $\Phi_1 = -\Phi_2 = l\varphi + \varphi_0$ in Eq. (1), the output beam is represented as a two-dimensional vector with respect to the orthonormal circular polarization basis $\{|\boldsymbol{R}_l\rangle, |\boldsymbol{L}_l\rangle\}$, such that

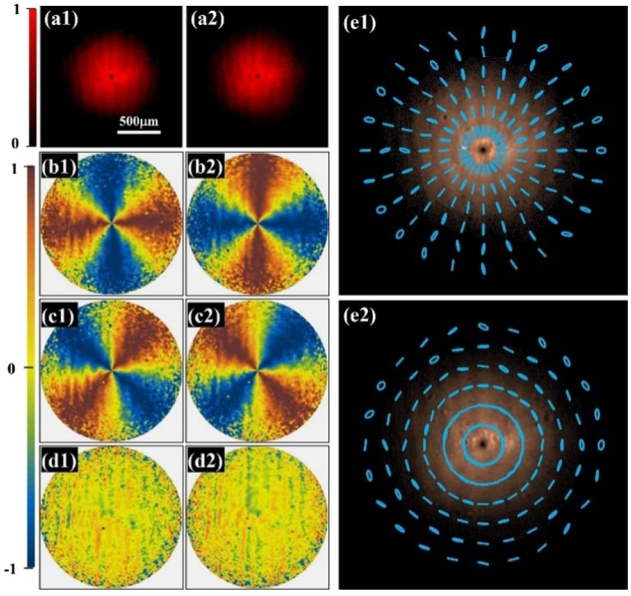

Fig. 2. Intensity and polarization distributions of the radially (1) and azimuthally (2) polarized beams. (a) Light intensity distributions captured by CCD, (b)–(d) measurement results of normalized Stokes parameters (S_1, S_2, S_3), and (e) polarization ellipse distributions.

$$|\boldsymbol{E}\rangle = \cos 2\theta e^{i\varphi_0}|\boldsymbol{R}_l\rangle + \sin 2\theta e^{-i\varphi_0}|\boldsymbol{L}_l\rangle, \quad (5)$$

where $|\boldsymbol{R}_l\rangle = \exp(il\varphi)\boldsymbol{e}_R$, and $|\boldsymbol{L}_l\rangle = \exp(-il\varphi)\boldsymbol{e}_L$. The above equation describes an arbitrary polarization state on the higher order Poincaré sphere [13,15], where the latitude and longitude can be controlled by the parameters θ and φ_0, respectively. Figure 3(a) shows a typical higher order Poincaré sphere for $l = 1$. When $\theta = \pi/8$, the polarization of the vector beam is located on the equator, e.g., $\varphi_0 = 0$ and $\pi/2$ correspond to the radially ($|\boldsymbol{H}_1\rangle$) and azimuthally ($|\boldsymbol{V}_1\rangle$) polarized beams, respectively, while $\theta = 0$ and $\pi/4$ correspond to the right

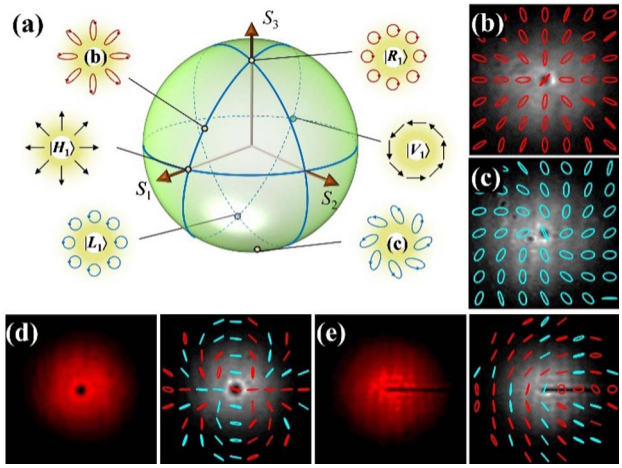

Fig. 3. Generated vector beams on a higher order Poincaré sphere. (a) Schematic of polarizations on a higher order Poincaré sphere for $l = 1$; (b), (c) experimental results of the generated vector beams for $\theta = 0.08\pi$, $\varphi_0 = 0$ and $\theta = 0.2\pi$, $\varphi_0 = \pi/6$, respectively; (d), (e) vector beams for $l = 2$ and 1/2, respectively, while $\theta = 0$, $\varphi_0 = 0$.

($|\boldsymbol{R}_1\rangle$) and left ($|\boldsymbol{L}_1\rangle$) circular polarizations, respectively, as also shown in Fig. 3(a).

We set $\theta = 0.08\pi$, $\varphi_0 = 0$ and $\theta = 0.2\pi$, $\varphi_0 = \pi/6$, respectively, and generate the vector beams on the higher order Poincaré sphere for $l = 1$. The corresponding results of measured polarizations are depicted in Figs. 3(b) and 3(c), where the red and cyan ellipses denote right ($S_3 > 0$) and left ($S_3 < 0$) elliptical polarizations, respectively. It can be clearly seen that the experimental results of these two vector beams are in accordance with the theoretical forms shown in the inset of Fig. 3(a).

Furthermore, the vector beams for the other orders, e.g., $l = 2$ and 1/2, can also be produced as shown in Figs. 3(d) and 3(e), respectively. The experimental results represent well the polarizations of orders $l = 2$ and 1/2, where the appearance of the red and cyan ellipses is the result of measurement errors. Notably, there are a dark core [Fig. 3(d)] and a dark line [Fig. 3(e)] in the intensity distributions of the vector beams, due to the singularity of polarizations. Thus, the displayed polarizations at these positions are insignificant.

C. Generating Arbitrary Vector Beams

We can generate a presupposed vector beam with an arbitrary polarization distribution just by loading a calculated phase map on the SLM. For example, the vector beams with multiple polarization singularities can be created by setting [50]

$$\Phi_1 = -\Phi_2 = \sum_{n=1}^{N} m_n \varphi_n + \varphi_0, \tag{6}$$

where N is the number of singularity, m_n and φ_n are the topological charge and azimuthal coordinate of the nth singularity at position (x_n, y_n), respectively, and $\varphi_n = \arg[(x - x_n) + i(y - y_n)]$ is satisfied. Figure 4 shows the experimental results of the generated vector beams with double singularities, where Figs. 4(a) and 4(b) correspond to $m_1 = m_2 = 1$ and $m_1 = -m_2 = 1$, respectively. In consideration of the local linear polarizations of these vector beams ($\theta = \pi/8$), the polarization ellipticity (or Stokes parameter S_3) can be ignored. To visualize in detail the polarization variation in space, the orientation distributions of the polarizations are calculated with the experimental data, and are depicted in the bottom of Fig. 4.

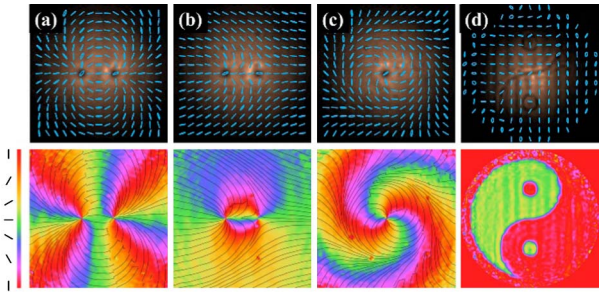

Fig. 4. Experimental results of the generated arbitrary vector beams. (a), (b) Vector beams with double singularities, (c) vector beam with radially and azimuthally varied polarization, and (d) vector beam with taiji-shaped polarization distribution. Top: measured polarization distributions. Bottom: corresponding orientation distributions of polarizations.

These experiment results represent the predicted polarizations well. Figures 4(c) and 4(d) are another two examples of vector beams with designed polarizations, which depict the radially and azimuthally varied polarization ($\Phi_1 = -\Phi_2 = \varphi + 2\pi r/r_0 + \pi/6$, $r_0 = 1.4$ mm) and taiji-shaped polarization, respectively.

D. Attaching Additional Phase to Vector Beams

According to Eq. (4), the generated vector beams can be attached with an additional phase by setting $\Phi_1 \neq -\Phi_2$. These vector beams are intuitively associated with the hybrid-order Poincaré sphere [14,51]. If $\Phi_1 = l\varphi + \varphi_0$, $\Phi_2 = m\varphi - \varphi_0$, the resulting field of the setup would represent a vector beam at the sphere coordinate $(2\varphi_0, \pi/2 - 4\theta)$ on the hybrid-order Poincaré sphere of order (l, m). Figures 5(a) and 5(b) show the experimental results of the vector beams $|\boldsymbol{H}_{0,-2}\rangle$ ($\varphi_0 = 0$, $\theta = \pi/8$, $l = 0$, $m = -2$) and $|\boldsymbol{H}_{5,-1}\rangle$ ($\varphi_0 = 0$, $\theta = \pi/8$, $l = 5$, $m = -1$), respectively, where the top and bottom are the measurement results of the polarization and phase distributions by employing the PB-phase method, respectively. Theoretically, the vector beam $|\boldsymbol{H}_{l,m}\rangle$ has a polarization state with order $(l - m)/2$ and a phase distribution $(l + m)/2$. The results in Figs. 5(a) and 5(b) conform well to this theory.

In addition, the vector beam can be endowed with arbitrary phase rather than the spiral one. In Fig. 5(c), we attach a conical phase to a single-charged vector beam. The parameters are set as $\theta = \pi/8$, and $\Phi_{1,2} = -2\pi r/260\ \mu\text{m} \pm (\varphi + \pi/6)$. The measurement results of the generated vector beam reveal the characteristics of cylindrical polarization and conical phase.

E. Tuning Amplitude of Vector Beams

Considering that the amplitude information can be encoded into the phase map [52], the amplitude of the generated vector beam can be conveniently tuned just through replacing the phase map on the SLM by a calculated one, which combines both the amplitude and phase information. Namely, if the vector beam to be produced is expressed by $E_0 \exp(i\Psi) \cdot [\cos\Theta, \sin\Theta]^T$, where E_0, Ψ, and Θ are, respectively, the amplitude, phase, and polarization direction, the phase patterns loaded on the SLM can be calculated by

$$\Phi_{1,2} = (1 - \sin c^{-1} E_0)\,\mathrm{mod}(\Psi \pm \Theta + \varphi_g, 2\pi), \tag{7}$$

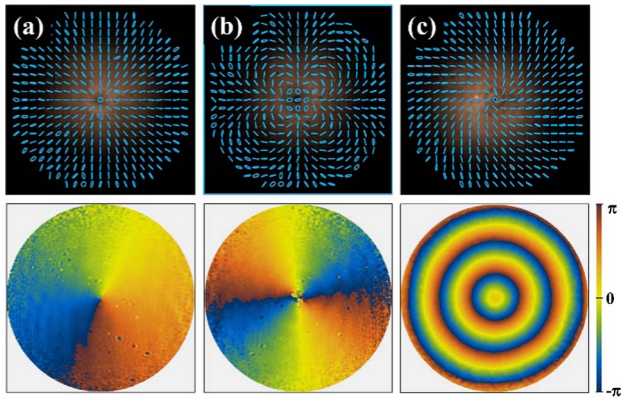

Fig. 5. Generated vector beams (top) and their phase distributions (bottom). (a) $\Theta = \varphi$, $\Psi = -\varphi$; (b) $\Theta = 3\varphi$, $\Psi = 2\varphi$; (c) $\Theta = \varphi + \pi/6$, $\Psi = -2\pi r/260$ μm.

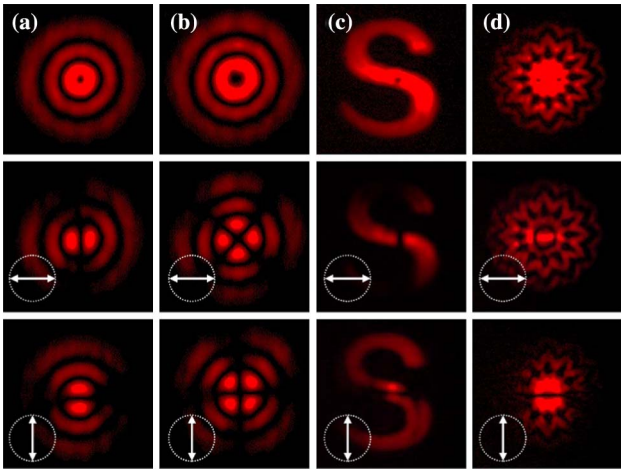

Fig. 6. Amplitude modulation of vector beams. (a), (b) Vector beams of Laguerre–Gaussian modes, (c) radially polarized S-shaped beam, and (d) flower-shaped vector beam with double singularities.

where $\varphi_g = k_x x$ induces a phase grating. A spatial filter at the focal plane of the imaging lens is needed to let only the first order pass through.

Figures 6(a) and 6(b) depict the generated vector beams of Laguerre–Gaussian modes $LG_{2,1}$ and $LG_{2,2}$, where the top panels are the intensity distributions on the imaging plane captured by CCD; the middle and bottom panels show the corresponding intensities after passing through the horizontal and vertical analyzers. As can be seen from the experimental results, three ring-like lobes appear in the rotationally symmetric intensity distributions, and the fanlike extinction patterns after using analyzers show the polarizations of vector beams with orders 1 and 2 for Figs. 6(a) and 6(b), respectively.

We can also encode arbitrary patterns into the phase maps, such as a letter "S" or a flower-shaped pattern, and generate vector beams with the corresponding intensity distributions. The results are shown in Figs. 6(c) and 6(d), where the polarizations are tuned as the radial one and the one with double singularities, respectively. An interesting pattern variation can be observed when the flower-shaped vector beam passes through a rotating analyzer, as also shown in Visualization 1.

It is important to note that the amplitude-encoded technology would reduce the energy of the first diffraction order, which depends on the amplitude distribution, inducing lower generation efficiency.

4. CONCLUSION

We propose an optical arrangement to efficiently generate tunable vector beams by employing a single phase-type SLM. With this arrangement, a linearly polarized Gaussian beam is converted into a vector beam, of which the polarization ellipticity, orientation, and distribution can be arbitrarily controlled, while an additional phased term is also granted. The energy loss of this arrangement is greatly reduced, which depends mainly on the reflectivity of the SLM. Accordingly, the conversion efficiency is substantially improved. Based on the measurements of the polarization and phase of the resulting fields via the PB-phase method, we experimentally demonstrate the generation of vector beams with cylindrical polarizations, on a higher order Poincaré sphere, with arbitrary polarizations, attached with phase, and with tunable amplitude. The proposed method is expected to create high-power vector beams and play important roles in optical fabrication and light trapping.

Funding. National Key Research and Development Program of China (2017YFA0303800); Joint Fund of the National Natural Science Foundation Committee of China Academy of Engineering Physics (CAEP) (U1630125); National Natural Science Foundation of China (NSFC) (11634010, 61675168, 11774289).

[†]These authors contributed equally to this work.

REFERENCES

1. M. Christian, J. Alexander, F. Severin, B. Stefan, and R.-M. Monika, "Tailoring of arbitrary optical vector beams," New J. Phys. **9**, 78 (2007).
2. Q. Zhan, "Cylindrical vector beams: from mathematical concepts to applications," Adv. Opt. Photonics **1**, 1–57 (2009).
3. S. Quabis, R. Dorn, M. Eberler, O. Glöckl, and G. Leuchs, "Focusing light to a tighter spot," Opt. Commun. **179**, 1–7 (2000).
4. R. Dorn, S. Quabis, and G. Leuchs, "Sharper focus for a radially polarized light beam," Phys. Rev. Lett. **91**, 233901 (2003).
5. H. Wang, L. Shi, B. Lukyanchuk, C. Sheppard, and C. T. Chong, "Creation of a needle of longitudinally polarized light in vacuum using binary optics," Nat. Photonics **2**, 501–505 (2008).
6. Y. Kozawa and S. Sato, "Focusing property of a double-ring-shaped radially polarized beam," Opt. Lett. **31**, 820–822 (2006).
7. Y. Zhao, Q. Zhan, Y. Zhang, and Y.-P. Li, "Creation of a three-dimensional optical chain for controllable particle delivery," Opt. Lett. **30**, 848–850 (2005).
8. X. Jiao, S. Liu, Q. Wang, X. Gan, P. Li, and J. Zhao, "Redistributing energy flow and polarization of a focused azimuthally polarized beam with rotationally symmetric sector-shaped obstacles," Opt. Lett. **37**, 1041–1043 (2012).
9. W. Zhang, S. Liu, P. Li, X. Jiao, and J. Zhao, "Controlling the polarization singularities of the focused azimuthally polarized beams," Opt. Express **21**, 974–983 (2013).
10. P. Li, S. Liu, G. Xie, T. Peng, and J. Zhao, "Modulation mechanism of multi-azimuthal masks on the redistributions of focused azimuthally polarized beams," Opt. Express **23**, 7131–7139 (2015).
11. Y. Zhang, P. Li, S. Liu, L. Han, H. Cheng, and J. Zhao, "Manipulating spin-dependent splitting of vector abruptly autofocusing beam by encoding cosine-azimuthal variant phases," Opt. Express **24**, 28409–28418 (2016).
12. X. Wang, J. Chen, Y. Li, J. Ding, C. Guo, and H. Wang, "Optical orbital angular momentum from the curl of polarization," Phys. Rev. Lett. **105**, 253602 (2010).
13. G. Milione, H. Sztul, D. Nolan, and R. Alfano, "Higher-order Poincaré sphere, Stokes parameters, and the angular momentum of light," Phys. Rev. Lett. **107**, 053601 (2011).
14. X. Yi, Y. Liu, X. Ling, X. Zhou, Y. Ke, H. Luo, S. Wen, and D. Fan, "Hybrid-order Poincaré sphere," Phys. Rev. A **91**, 023801 (2015).
15. G. Milione, S. Evans, D. A. Nolan, and R. R. Alfano, "Higher order Pancharatnam-Berry phase and the angular momentum of light," Phys. Rev. Lett. **108**, 190401 (2012).
16. S. Liu, M. Wang, P. Li, P. Zhang, and J. Zhao, "Abrupt polarization transition of vector autofocusing Airy beams," Opt. Lett. **38**, 2416–2418 (2013).
17. S. Liu, P. Li, Y. Zhang, X. Gan, M. Wang, and J. Zhao, "Longitudinal spin separation of light and its performance in three-dimensionally controllable spin-dependent focal shift," Sci. Rep. **6**, 20774 (2016).

18. J. Zhou, W. Zhang, Y. Liu, Y. Ke, Y. Liu, H. Luo, and S. Wen, "Spin-dependent manipulating of vector beams by tailoring polarization," Sci. Rep. **6**, 34276 (2016).
19. B. Wei, P. Chen, W. Hu, W. Ji, L. Zheng, S. Ge, Y. Ming, V. Chigrinov, and Y. Lu, "Polarization-controllable Airy beams generated via a photoaligned director-variant liquid crystal mask," Sci. Rep. **5**, 17484 (2015).
20. F. Cardano and L. Marrucci, "Spin-orbit photonics," Nat. Photonics **9**, 776–778 (2015).
21. X. Ling, X. Yi, X. Zhou, Y. Liu, W. Shu, H. Luo, and S. Wen, "Realization of tunable spin-dependent splitting in intrinsic photonic spin Hall effect," Appl. Phys. Lett. **105**, 151101 (2014).
22. Y. Zhang, P. Li, S. Liu, and J. Zhao, "Unveiling the photonic spin Hall effect of freely propagating fan-shaped cylindrical vector vortex beams," Opt. Lett. **40**, 4444–4447 (2015).
23. Q. Zhan, "Trapping metallic Rayleigh particles with radial polarization," Opt. Express **12**, 3377–3382 (2004).
24. T. A. Nieminen, N. R. Heckenberg, and H. Rubinsztein-Dunlop, "Forces in optical tweezers with radially and azimuthally polarized trapping beams," Opt. Lett. **33**, 122–124 (2008).
25. X. Xie, Y. Chen, K. Yang, and J. Zhou, "Harnessing the point-spread function for high-resolution far-field optical microscopy," Phys. Rev. Lett. **113**, 263901 (2014).
26. D. P. Biss, K. S. Youngworth, and T. G. Brown, "Dark-field imaging with cylindrical-vector beams," Appl. Opt. **45**, 470 (2006).
27. C. Hnatovsky, V. Shvedov, W. Krolikowski, and A. Rode, "Revealing local field structure of focused ultrashort pulses," Phys. Rev. Lett. **106**, 123901 (2011).
28. C. Loussert and E. Brasselet, "Efficient scalar and vectorial singular beam shaping using homogeneous anisotropic media," Opt. Lett. **35**, 7–9 (2010).
29. Y. Kozawa and S. Sato, "Generation of a radially polarized laser beam by use of a conical Brewster prism," Opt. Lett. **30**, 3063–3065 (2005).
30. G. Machavariani, Y. Lumer, I. Moshe, A. Meir, and S. Jackel, "Efficient extracavity generation of radially and azimuthally polarized beams," Opt. Lett. **32**, 1468–1470 (2007).
31. L. Marrucci, C. Manzo, and D. Paparo, "Optical spin-to-orbital angular momentum conversion in inhomogeneous anisotropic media," Phys. Rev. Lett. **96**, 163905 (2006).
32. Z. Bomzon, G. Biener, V. Kleiner, and E. Hasman, "Radially and azimuthally polarized beams generated by space-variant dielectric subwavelength gratings," Opt. Lett. **27**, 285–287 (2002).
33. F. Yue, D. Wen, J. Xin, B. D. Gerardot, J. Li, and X. Chen, "Vector vortex beam generation with a single plasmonic metasurface," ACS Photon. **3**, 1558–1563 (2016).
34. Y. Liu, X. Ling, X. Yi, X. Zhou, H. Luo, and S. Wen, "Realization of polarization evolution on higher-order Poincaré sphere with metasurface," Appl. Phys. Lett. **104**, 191110 (2014).
35. M. M. Sánchez-López, J. A. Davis, N. Hashimoto, I. Moreno, E. Hurtado, K. Badham, A. Tanabe, and S. W. Delaney, "Performance of a q-plate tunable retarder in reflection for the switchable generation of both first- and second-order vector beams," Opt. Lett. **41**, 13–16 (2016).
36. Z. Liu, Y. Liu, Y. Ke, Y. Liu, W. Shu, H. Luo, and S. Wen, "Generation of arbitrary vector vortex beams on hybrid-order Poincaré sphere," Photon. Res. **5**, 15–21 (2017).
37. D. Naidoo, F. S. Roux, A. Dudley, I. Litvin, B. Piccirillo, L. Marrucci, and A. Forbes, "Controlled generation of higher-order Poincaré sphere beams from a laser," Nat. Photonics **10**, 327–332 (2016).
38. X. L. Wang, J. Ding, W. J. Ni, C. S. Guo, and H. T. Wang, "Generation of arbitrary vector beams with a spatial light modulator and a common path interferometric arrangement," Opt. Lett. **32**, 3549–3551 (2007).
39. P. H. Jones, M. Rashid, M. Makita, and O. M. Maragò, "Sagnac interferometer method for synthesis of fractional polarization vortices," Opt. Lett. **34**, 2560–2562 (2009).
40. H. Chen, J. Hao, B. F. Zhang, J. Xu, J. Ding, and H. T. Wang, "Generation of vector beam with space-variant distribution of both polarization and phase," Opt. Lett. **36**, 3179–3181 (2011).
41. I. Moreno, J. A. Davis, D. M. Cottrell, and R. Donoso, "Encoding high-order cylindrically polarized light beams," Appl. Opt. **53**, 5493–5501 (2014).
42. S. Liu, P. Li, T. Peng, and J. Zhao, "Generation of arbitrary spatially variant polarization beams with a trapezoid Sagnac interferometer," Opt. Express **20**, 21715–21721 (2012).
43. S. Chen, X. Zhou, Y. Liu, X. Ling, H. Luo, and S. Wen, "Generation of arbitrary cylindrical vector beams on the higher order Poincaré sphere," Opt. Lett. **39**, 5274–5276 (2014).
44. P. Li, Y. Zhang, S. Liu, C. Ma, L. Han, H. Cheng, and J. Zhao, "Generation of perfect vectorial vortex beams," Opt. Lett. **41**, 2205–2208 (2016).
45. Y. Zhang, P. Li, C. Ma, S. Liu, H. Cheng, L. Han, and J. Zhao, "Efficient generation of vector beams by calibrating the phase response of a spatial light modulator," Appl. Opt. **56**, 4956–4960 (2017).
46. S. Li, S. Qian, L. Kong, Z. Ren, Y. Li, C. Tu, and H. Wang, "An efficient and robust scheme for controlling the states of polarization in a Sagnac interferometric configuration," Europhys. Lett. **105**, 64006 (2014).
47. U. Ruiz, P. Pagliusi, C. Provenzano, and G. Cipparrone, "Highly efficient generation of vector beams through polarization holograms," Appl. Phys. Lett. **102**, 161104 (2013).
48. S. Liu, L. Han, P. Li, Y. Zhang, H. Cheng, and J. Zhao, "A method for simultaneously measuring polarization and phase of arbitrarily polarized beams based on Pancharatnam-Berry phase," Appl. Phys. Lett. **110**, 171112 (2017).
49. H. Cheng, P. Li, S. Liu, P. Chen, L. Han, Y. Zhang, W. Hu, and J. Zhao, "Vortex-controlled morphology conversion of microstructures on silicon induced by femtosecond vector vortex beams," Appl. Phys. Lett. **111**, 141901 (2017).
50. L. Han, S. Liu, P. Li, Y. Zhang, H. Cheng, X. Gan, and J. Zhao, "Managing focal fields of vector beams with multiple polarization singularities," Appl. Opt. **55**, 9049–9053 (2016).
51. Y. Liu, Z. Liu, J. Zhou, X. Ling, W. Shu, H. Luo, and S. Wen, "Measurements of Pancharatnam-Berry phase in mode transformations on hybrid-order Poincaré sphere," Opt. Lett. **42**, 3447–3450 (2017).
52. J. A. Davis, D. M. Cottrell, J. Campos, M. J. Yzuel, and I. Moreno, "Encoding amplitude information onto phase-only filters," Appl. Opt. **38**, 5004–5013 (1999).